Reflectance and Fluorescent Spectra Recovery based on Fluorescent Chromaticity Invariance under Varying Illumination

Ying Fu
The University of Tokyo
fuying@iis.u-tokyo.ac.jp

Antony Lam
National Institute of Informatics
antony@nii.ac.jp

Yasuyuki Kobashi
Ministry of Internal
Affairs and Communications
koba0132.poke@gmail.com

Imari Sato
National Institute of Informatics
imarik@nii.ac.jp

Takahiro Okabe
Kyushu Institute of Technology
okabe@ai.kyutech.ac.jp

Yoichi Sato
The University of Tokyo
ysato@iis.u-tokyo.ac.jp

Abstract

In recent years, fluorescence analysis of scenes has received attention. Fluorescence can provide additional information about scenes, and has been used in applications such as camera spectral sensitivity estimation, 3D reconstruction, and color relighting. In particular, hyperspectral images of reflective-fluorescent scenes provide a rich amount of data. However, due to the complex nature of fluorescence, hyperspectral imaging methods rely on specialized equipment such as hyperspectral cameras and specialized illuminants. In this paper, we propose a more practical approach to hyperspectral imaging of reflective-fluorescent scenes using only a conventional RGB camera and varied colored illuminants. The key idea of our approach is to exploit a unique property of fluorescence: the chromaticity of fluorescence emissions are invariant under different illuminants. This allows us to robustly estimate spectral reflectance and fluorescence emission chromaticity. We then show that given the spectral reflectance and fluorescent chromaticity, the fluorescence absorption and emission spectra can also be estimated. We demonstrate in results that all scene spectra can be accurately estimated from RGB images. Finally, we show that our method can be used to accurately relight scenes under novel lighting.

1. Introduction

Fluorescence analysis has received attention in recent years. This is because fluorescence can provide additional information about scenes and has been applied to problems in camera spectral sensitivity estimation [5], 3D reconstruction [16, 18], immersion range scanning [6], and color relighting [10, 4] to name a few. In particular, hyperspec-
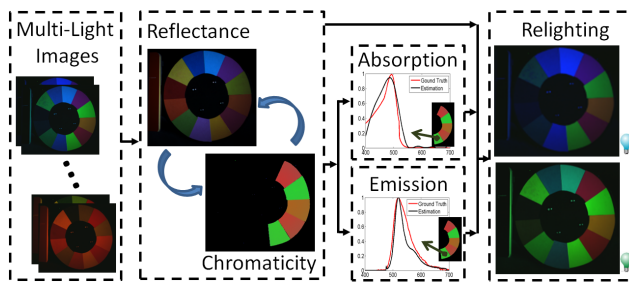

Figure 1. Overview of the method. The input images are captured under varied illuminants. The reflectance spectrum and the chromaticity of the fluorescent component are optimized in a process of alternating iterations that exploits the illuminant-invariant chromaticity of fluorescence. After that, the fluorescence absorption and emission spectra are estimated.

tral images of reflective-fluorescent scenes provides a rich amount of data.

However, capturing such hyperspectral reflective-fluorescent images is challenging due to the very different ways that reflectance and fluorescence responds to incident light [9, 20]. When a reflective surface is illuminated at a particular wavelength, it reflects back light of the same wavelength. For a fluorescent surface, light is absorbed at certain wavelengths and then light is emitted back at other wavelengths. Therefore a fluorescence imaging system needs to be able to capture the relationship between absorption and emission wavelengths.

The conventional approach to capturing this relationship is to exhaustively measure different combinations of absorbing and emitting wavelengths [11]. This is labor intensive and only works for a single surface point. Thus it is impractical for imaging entire scenes.

Instead, a camera based solution where entire scenes can be captured would be desirable. Zhang and Sato [20] proposed a method that uses a RGB camera and ICA to separate

1

reflective and fluorescent components but their method does not capture spectral distributions. In recent work, methods for hyperspectral imaging of reflective-fluorescent scenes have been proposed [10, 4]. These methods are effective but require specialized cameras and specialized illuminants such as narrowband light or high frequency light spectra.

We propose a more practical approach to hyperspectral imaging of reflective-fluorescent scenes using only a conventional RGB camera and varied colored illuminants. Our method takes as input RGB images under different lighting and effectively separates reflectance and fluorescence in the spectral domain. These separated results can then be used for tasks such as accurate color relighting of scenes under novel lighting (Figure 1).

The key idea in our approach is to exploit a unique property of fluorescence: the chromaticity of fluorescence emissions are invariant under different illuminants. Based on this property, we formulate a method that takes RGB images and performs pixel-wise estimation of spectral reflectance and fluorescent chromaticity. The method works by iteratively improving estimates of the spectral reflectance and fluorescent chromaticity in turn. We show our method is robust to initialization conditions and converges onto accurate spectral reflectance and fluorescent chromaticity for real scenes. Then we propose methods for estimating the fluorescence absorption and emission spectra of the scene given the estimated spectral reflectance data and fluorescent chromaticities.

In summary, our main contributions are that we

1. Exploit the illuminant-invariant chromaticity of fluorescence to estimate both spectral reflectance and fluorescent chromaticity from RGB images,
2. Devise a means for estimating fluorescence absorption and emission spectra from given spectral reflectance and fluorescent chromaticity,
3. Ultimately, presenting the first system capable of imaging all reflective and fluorescence absorption and emission spectra of real scenes using only a conventional RGB camera and varied colored illuminants.

We show our method is accurate and demonstrate its effectiveness in predicting color relighting of real scenes.

2. Related Work

A number of methods for capturing only the spectral reflectance of scenes using conventional RGB cameras have been proposed [3, 12, 8]. These methods are practical and effective for imaging spectral reflectance but their limitation is they cannot accurately capture scenes with fluorescent surfaces. The reason for this loss in accuracy is because reflective and fluorescent surfaces react to incident light very differently.

The detrimental effects of not considering fluorescence is nicely illustrated in Johnson and Fairchild [9] where they showed that taking fluorescence into account dramatically improved color renderings. Furthermore, Barnard proposed improvements to color constancy algorithms which included spectral data from several fluorescent materials [2]. Later, Wilkie *et al.* [19] showed accurate results by rendering fluorescence emissions using diffuse surfaces that can reflect light at a wavelength different from its incident illuminant wavelength. Hullin *et al.* [7] also demonstrated the importance of modeling different reflective-fluorescent materials by introducing the bidirectional reflectance and reradiation distribution function (BRRDF).

A conventional way to measure fluorescence in the spectral domain is to use Bispectral measurements [11]. However, exhaustively measuring different combinations of absorption and emission wavelengths is labor intensive. In addition, such measurements only work for a single surface point. Thus they are impractical for imaging scenes.

Instead, a camera based approach is more desirable. Zhang and Sato [20] proposed an ICA based reflective-fluorescent separation method. Tominaga *et al.* [17] used two light sources and multispectral imaging to estimate fluorescence emission spectra. Alterman *et al.* separated the appearance of each fluorescent dye from a mixture by unmixing multiplexed images [1]. None of these methods fully recover all reflective and fluorescent components of scenes. In recent work, methods for hyperspectral imaging of reflective-fluorescent scenes have been proposed. Lam and Sato [10] provided a method for recovering the full spectral reflectance and fluorescence absorption and emission spectra of scenes but they require a multiband camera and multiple narrowband illuminants. Fu *et al.* [4] also recovered the full spectral reflectance and fluorescence spectra of scenes by using high frequency light spectra but they require a hyperspectral camera and a programmable light source: a device that can be programmed to produce arbitrary light spectra. While effective, these methods require specialized equipment so their use in applications is limited. We propose a more practical approach to fully capturing the reflectance and fluorescence absorption and emission spectra of scenes using a RGB camera and varied illuminants.

3. Reflectance and Fluorescence Spectra Estimation

3.1. Problem Formulation

We start by describing the basic formulation of our problem. When taking an image of a scene with reflective-fluorescent components using a RGB camera, the intensity of each pixel for the n-th channel under the m-th illuminant is

$$p_n^m = r_n^m + f_n^m. \tag{1}$$

r_n^m is the reflective component for the n-th channel under the m-th illuminant and can be described by

$$r_n^m = \int c_n(\lambda) l_m(\lambda) s(\lambda) \mathrm{d}\lambda, \qquad (2)$$

where $s(\lambda)$ is the spectral reflectance of the material at wavelength λ, $l_m(\lambda)$ is the m-th illuminant's intensity and $c_n(\lambda)$ ($n = 1, 2, 3$) is the corresponding camera spectral sensitivity for the R, G, and B channels.

f_n^m is the fluorescent component [20] for the n-th channel under the m-th illuminant and

$$f_n^m = \left(\int l_m(\lambda') a(\lambda') \mathrm{d}\lambda' \right) \int c_n(\lambda) e(\lambda) \mathrm{d}\lambda = k_m D_n \qquad (3)$$

where λ' and λ are the wavelengths of the incident light and the outgoing fluorescence emission respectively, $a(\lambda')$ and $e(\lambda)$ represent the absorption and emission spectra at their respective wavelengths, and $k_m = \int l_m(\lambda') a(\lambda') \mathrm{d}\lambda'$ and $D_n = \int c_n(\lambda) e(\lambda) \mathrm{d}\lambda$.

Substituting Equations (2) and (3) into Equation (1),

$$p_n^m = \int c_n(\lambda) l_m(\lambda) s(\lambda) \mathrm{d}\lambda \\ + \left(\int l_m(\lambda') a(\lambda') \mathrm{d}\lambda' \right) \int c_n(\lambda) e(\lambda) \mathrm{d}\lambda. \qquad (4)$$

Equation (4) describes how the components of a reflective-fluorescent surface jointly appear in a camera image under illuminant l_m. Our task is to determine the full spectral reflectance s and fluorescence absorption spectrum a and emission spectrum e given the observed p_n^m under different illuminants l_m and camera spectral sensitivity c_n, which can be estimated by

$$\{\hat{s}, \hat{a}, \hat{e}\} = \arg \min_{s,a,e} G(s, a, e), \qquad (5)$$

where

$$G(s, a, e) = \sum_m \sum_n \| p_n^m - \hat{p}_n^m(s, a, e) \|_2^2 \qquad (6)$$

and $\hat{p}_n^m(s, a, e)$ is the estimated parameterization of p_n^m.

Our method for optimizing Equation (5) makes use of the illuminant-invariant chromaticity of fluorescence. We now show how chromaticity value E_n^m of the fluorescent component under the m-th illuminant for the n-th channel can be computed. We define chromaticity as the normalized RGB fluorescence emission,

$$E_n^m = \frac{k_m D_n}{\sum_{t=1}^3 k_m D_t} = \frac{D_n}{\sum_{t=1}^3 D_t} = E_n, \qquad (7)$$

where E_n is called the reference chromaticity.

Equation (7) implies chromaticity value E_n^m is independent of its illuminant and is thus constant. We also note that

since $\sum_n^3 E_n = 1$, $E_3 = 1 - E_1 - E_2$, the chromaticity can be uniquely expressed with only 2 values. However, for convenience in our derivations, we will express chromaticity in terms of 3 values.

In summary, we will determine all spectral components in two stages. We start by using the illuminant-invariant chromaticity of fluorescence to estimate the reflectance spectrum s and the fluorescent chromaticity values E_n for all channels n. After that, the fluorescence absorption spectrum a and emission spectrum e can be recovered. Figure 1 shows an overview of the proposed method.

3.2. Reflectance Spectrum Recovery

In the previous sections, we described that the chromaticity of fluorescence is invariant under different illuminants. We now show how to use the illuminant-invariant chromaticity of fluorescence in conjunction with basis functions for spectral reflectance to estimate the spectral reflectance of the scene.

According to a previous study [15], the spectral reflectance of various materials can be approximately represented by using a small number of basis functions as

$$s(\lambda) = \sum_{j=1}^J \alpha_j b_j(\lambda), \qquad (8)$$

where $b_j(\lambda)(j = 1, 2, \cdots, J)$ are the basis functions for spectral reflectance and α_j are the corresponding coefficients. From Equation (8), Equation (2) can be rewritten as

$$r_n^m = \sum_j \alpha_j \int c_n(\lambda) l_m(\lambda) b_j(\lambda) \mathrm{d}\lambda = \sum_j \alpha_j q_{n,j}^m, \quad (9)$$

where $q_{n,j}^m = \int c_n(\lambda) l_m(\lambda) b_j(\lambda) \mathrm{d}\lambda$.

We now show that the illuminant-invariant chromaticity of the fluorescence makes it possible to estimate the spectral reflectance s without knowing absorption spectrum a and emission spectrum e. First note that $f_n^m = p_n^m - r_n^m = p_n^m - \sum_j \alpha_j q_{n,j}^m$. According Equation (7), the chromaticity value E_n^m for channel n under illumination m can be computed by

$$E_n^m = \frac{f_n^m}{\sum_t f_t^m} = \frac{p_n^m - \sum_j \alpha_j q_{n,j}^m}{\sum_t (p_t^m - \sum_j \alpha_j q_{t,j}^m)} = E_n. \quad (10)$$

By straightforward algebraic manipulation of Equation (10), we can see that

$$p_n^m = E_n \sum_t (p_t^m - \sum_j \alpha_j q_{t,j}^m) + \sum_j \alpha_j q_{n,j}^m = p_n^m(\boldsymbol{\alpha}, \boldsymbol{E}). \qquad (11)$$

where $\boldsymbol{\alpha}$ is the set of coefficients $\alpha_j(j = 1, 2, ...J)$ and $\boldsymbol{E}$ is the set of chromaticity values $E_n(n = 1, 2, 3)$, and

$p_n^m(\boldsymbol{\alpha}, \boldsymbol{E})$ is the parameterization of p_n^m. Then instead of minimizing Equation (6), we can minimize

$$G(\boldsymbol{\alpha}, \boldsymbol{E}) = \sum_m \sum_n \|p_n^m - \hat{p}_n^m(\boldsymbol{\alpha}, E_n)\|_2^2, \quad (12)$$

where $\hat{p}_n^m(\boldsymbol{\alpha}, E_n)$ is called the estimated parameterization of p_n^m. Equation (12) shows that coefficients $\boldsymbol{\alpha}$ and chromaticity $\boldsymbol{E}$ can be estimated in place of $\boldsymbol{s}$, $\boldsymbol{a}$, and $\boldsymbol{e}$.

The parameters $\boldsymbol{\alpha}$ and $\boldsymbol{E}$ need to be chosen to minimize the error function in Equation (12). Determining $\boldsymbol{\alpha}$ would allow for recovering the spectral reflectance $\boldsymbol{s}$ according to Equation (8). Finding $\boldsymbol{E}$ would provide us with the fluorescent chromaticity which will be used in later steps to determine the fluorescence spectral components.

We propose a simple and effective method for estimating parameters $\boldsymbol{\alpha}$ and $\boldsymbol{E}$ using alternating iterations to converge upon a solution. We first initialize $\boldsymbol{E}$ to an approximation of the true emission chromaticity by setting it to be the average of the RGB values of the surface point imaged under the M illuminants. A more detailed discussion on the initialization of $\boldsymbol{E}$ can be found in Section 3.5. We then solve for $\boldsymbol{\alpha}$ as

$$\hat{\boldsymbol{\alpha}} = \arg \min_{\boldsymbol{\alpha}} \sum_m \sum_n \|p_n^m - \hat{p}_n^m(\boldsymbol{\alpha}, \boldsymbol{E})\|_2^2. \quad (13)$$

One way to solve Equation (13) is to find $\boldsymbol{\alpha}$ such that $p_n^m = \hat{p}_n^m(\boldsymbol{\alpha}, \boldsymbol{E}) = E_n \sum_t (p_t^m - \sum_{j=1}^J \alpha_j q_{t,j}^m) + \sum_{j=1}^J \alpha_j q_{n,j}^m$. Then rearranging terms in the equation, we can get

$$y_n^m = \sum_j \alpha_j w_{n,j}^m, \quad (14)$$

where $y_n^m = p_n^m - E_n \sum_t p_t^m$ and $w_{n,j}^m = q_{n,j}^m - E_n \sum_t q_{t,j}^m$. Equation (14) can be solved for all m and n in matrix form by finding the vector $\boldsymbol{\alpha} = [\alpha_1, ..., \alpha_J]^T$ such that

$$\boldsymbol{y} = \boldsymbol{W}\boldsymbol{\alpha}, \quad (15)$$

where $\boldsymbol{y} = [y_1^1, y_2^1, y_3^1, ..., y_1^M, y_2^M, y_3^M]^T$, is a $3M \times 1$ vector and $\boldsymbol{W}$ is a $3M \times J$ matrix where $\boldsymbol{W}_{3(m-1)+n,j} = w_{n,j}^m$.

In our system, we actually have $2M$ independent equations because chromaticity is uniquely expressed in only 2 values. We choose M, such that $2M > J$, so the problem of estimating coefficients $\boldsymbol{\alpha}$ is over-determined. We adopted the constrained minimization method employed in Park *et al.* [14] with a non-negative constraint on the reconstructed reflectance spectrum and use the second derivative of the reflectance spectrum with respect to λ as a smoothness constraint,

$$\hat{\boldsymbol{\alpha}} = \arg \min \left\{ \|\boldsymbol{y} - \boldsymbol{W}\boldsymbol{\alpha}\|_2^2 + \mu_r \int \left(\frac{\partial^2 s(\lambda)}{\partial \lambda^2} \right)^2 \mathrm{d}\lambda \right\},$$
$$s.t. \quad \boldsymbol{B}\boldsymbol{\alpha} \geq 0 \quad \text{for all } \lambda, \quad (16)$$

where μ_r is a weight for the constraint term. $\boldsymbol{B}$'s columns are the reflectance spectral basis vectors b_m.

Given the estimated $\boldsymbol{\alpha}$, $\boldsymbol{E}$ can be estimated by minimizing the same error function in Equation (12) with the constraint that $\sum_n^3 E_n = 1$. After several alternating iterations between estimating $\boldsymbol{\alpha}$ and $\boldsymbol{E}$, we converge upon a solution where $\boldsymbol{\alpha}$ and $\boldsymbol{E}$ are well estimated. With $\boldsymbol{\alpha}$ estimated, spectral reflectance $\boldsymbol{s}$ can be reconstructed by Equation (8).

3.3. Fluorescence Absorption Spectrum Recovery

Using the obtained spectral reflectance $\boldsymbol{s}$ and Equation (2), the appearance of the fluorescent component under the m-th illuminant is computed as $f_n^m = p_n^m - r_n^m$ and we will describe how the fluorescence spectral components can be estimated given f_n^m.

Previous work has also shown that absorption spectra can be well represented by basis functions [10]. In our investigation, we have found that a large collection of absorption spectra from the McNamara and Boswell Fluorescence Spectral Dataset [13] can be well represented using 9 principal components. Thus our observed absorption spectrum can be expressed as a linear combination of basis vectors

$$a(\lambda) = \sum_{i=1}^9 \beta_i v_i(\lambda), \quad (17)$$

where $v_i(\lambda)$ ($i = 1, \cdots, 9$) is the i-th basis vector at wavelength λ and β_i is the corresponding coefficient. From Equations (3) and (17) the fluorescent component f_n^m can be described as

$$f_n^m = D_n \sum_i \beta_m \int l_m(\lambda) v_i(\lambda) \mathrm{d}\lambda = D_n \sum_i \beta_m h_i^m$$
$$= \gamma E_n \sum_i \beta_m h_i^m \quad (18)$$

where $h_i^m = \int l_m(\lambda) v_i(\lambda) \mathrm{d}\lambda$ and $\gamma = \sum_{t=1}^3 D_t$.

E_n was determined from Section 3.2 so it can be used to recover the fluorescence absorption spectrum by estimating the coefficients β_i as

$$\hat{\boldsymbol{\beta}} = \arg \min_{\boldsymbol{\beta}} \sum_m \sum_n \|f_n^m - \gamma E_n \sum_i \beta_i h_i^m\|_2^2. \quad (19)$$

Similarly to Equation (16), this is solved with a regularization term as

$$\hat{\boldsymbol{\beta}} = \arg \min \left\{ \|\boldsymbol{f} - \boldsymbol{H}\boldsymbol{\beta}\|_2^2 + \mu_a \int \left(\frac{\partial^2 a(\lambda)}{\partial \lambda^2} \right)^2 \mathrm{d}\lambda \right\},$$
$$s.t. \quad \boldsymbol{V}\boldsymbol{\beta} \geq 0 \quad \text{for all } \lambda, \quad (20)$$

where $\boldsymbol{f} = [f_1^1, \cdots, f_3^M]^T$, is a $3M \times 1$ vector, $\boldsymbol{\beta} = \gamma[\beta_1, \cdots, \beta_9]^T$ is a 9×1 coefficient vector, and $\boldsymbol{H}$ is a
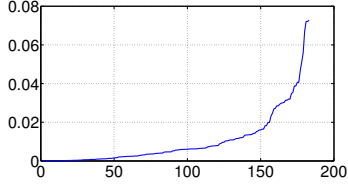
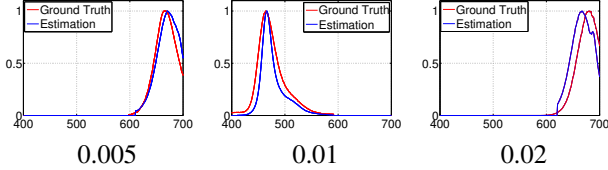Figure 2. All test errors sorted in ascending order. 69% of cases were below the average error of 0.01.

0.005	0.01	0.02

Figure 3. Examples of estimated emission spectra and their root-mean-square-errors.

matrix where $\boldsymbol{H}^m_{3(m-1)+n,i} = h^m_i E_n$. $\boldsymbol{V}$ is a matrix whose columns are the absorption spectral basis vectors and γ is just a scale factor that does not affect the estimated shape of the fluorescence absorption spectrum. With the calculated results by Equation (20), the fluorescence absorption spectrum can be recovered by Equation (17).

3.4. Fluorescence Emission Spectrum Recovery

In our system, we use a RGB camera to capture the scene and only have 2 values for the fluorescent chromaticity $\boldsymbol{E}$ to recover the emission spectrum. Estimating an entire emission spectrum from only 2 values is a challenging problem but we have devised a data driven method that is effective. We observe the emission spectra in the McNamara and Boswell Fluorescence Spectral Dataset, and find they all have similar bell shapes (see Figure 3 for examples) but with different widths and peaks at different wavelengths. Due to the restricted types of shapes exhibited by emission spectra, we have found that similar emission chromaticities generally map to similar emission spectra.

This makes it possible to determine the corresponding emission spectrum to a given emission chromaticity by performing a simple procedure. We use the known camera spectral sensitivity and integrate it with each fluorescence emission spectrum in the dataset to obtain the corresponding chromaticity for each fluorescence emission. Then, we compare the estimated fluorescent chromaticity $\boldsymbol{E}$ with the fluorescent chromaticities from the dataset. The dataset emission spectrum's chromaticity with the lowest sum square error to the estimated fluorescent chromaticity $\boldsymbol{E}$ is then chosen as $\boldsymbol{E}$'s emission spectrum.

To test the effectiveness of our method, we conducted tests on the McNamara and Boswell Fluorescence Spectral Dataset. We first chose a subset of materials such that the emission and absorption spectra were both present in the visible spectrum (400 - 700 nm).[1] This resulted in a col-

Sheets	Average Chromaticity	Standard Deviation	Ground Truth	Average Image
Pink	(0.61, 0.19)	(0.01, 0.00)	(0.61 0.20)	(0.62, 0.14)
Green	(0.15, 0.64)	(0.01, 0.02)	(0.16 0.64)	(0.15, 0.69)
Orange	(0.56, 0.32)	(0.02, 0.02)	(0.56 0.31)	(0.56, 0.30)
Red	(0.61, 0.21)	(0.00, 0.00)	(0.61 0.20)	(0.65, 0.16)
Yellow	(0.19, 0.62)	(0.01, 0.03)	(0.19 0.62)	(0.19, 0.68)

Table 1. Average and standard deviations of the converged upon estimated chromaticities under all 66 initializations of $\boldsymbol{E}$. The 66 initializations are densely and uniformly distributed in the space of possible initializations of $\boldsymbol{E}$. The low standard deviations indicate our estimation method is robust to different initializations of $\boldsymbol{E}$. The last column shows the results from using the average RGB values of the input images to our procedure to initialize $\boldsymbol{E}$.

lection of 183 materials. We then tested our method using leave-one-out cross-validation on the 183 emission spectra. In each case, the error between the estimated emission spectrum and its ground truth was computed using the root-mean-square-error (RMSE). Before computing the errors, the estimation and ground truth were also normalized for scale by setting them to be unit length vectors.

In our results, we found an average error of 0.01. See Figure 2 for a plot of all the errors for the 183 estimated emission spectra. Our results indicate that the majority of materials fit our assumption and emission spectra are accurately estimated as can be seen in Figure 3. We did find cases with higher errors that violated our assumption but these cases only constituted a small set.

3.5. Fluorescent Chromaticity Initialization

In Equation (13), to estimate the reflectance spectrum, we need to initialize the chromaticity $\boldsymbol{E}$ of the fluorescent component first. In our method, we initialized $\boldsymbol{E}$ by the average of the RGB values of the pixel imaged under the M illuminants. This choice was based on the reasoning that since only the fluorescent component would have constant chromaticity over all illuminants, the average RGB value should be skewed towards the true fluorescent chromaticity.

We test the effectiveness of this idea against other possible initialization values for $\boldsymbol{E}$ by exhaustively trying different values for chromaticity and running our alternating iterations described in Section 3.2 to see what kinds of chromaticity values would be converged upon. For the types of initializations tested, we choose a dense and uniformly distributed set of initializations for $\boldsymbol{E}$ from the space of possible chromaticities. This amounted to 66 initializations.

Table 1 shows average estimated chromaticities and their standard deviations for all 66 initializations for the 5 fluorescent sheets on the color wheel in Figure 1. We found the averages in Table 1 to be close to the ground truth chromaticities. Initializing with the average RGB values from

---

[1]We chose this subset because our experimental setup is currently focused on imaging in the visible spectrum. Although conceptually, our methods would extend to non-visible wavelengths as well.
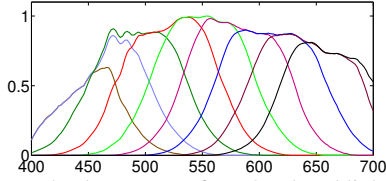
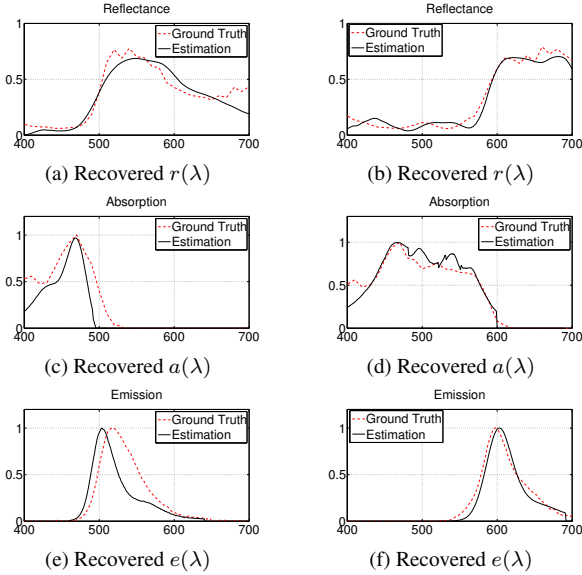Figure 4. The spectra of our 9 colored lights.

(a) Recovered $r(\lambda)$

(b) Recovered $r(\lambda)$

(c) Recovered $a(\lambda)$

(d) Recovered $a(\lambda)$

(e) Recovered $e(\lambda)$

(f) Recovered $e(\lambda)$

Figure 5. Recovered reflectance $r(\lambda)$, fluorescence absorption $a(\lambda)$ and emission $e(\lambda)$ spectra of the green and orange sheets. The left column is for the green sheet and the right column is for the orange sheet.

(a) Recovered $r(\lambda)$ (b) Recovered $a(\lambda)$ (c) Recovered $e(\lambda)$
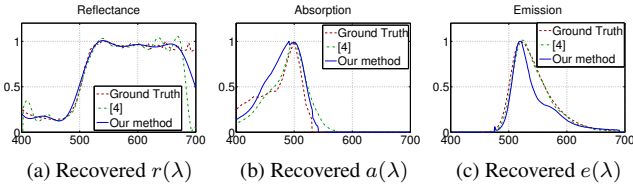
Figure 6. Comparison of [4] and our method using synthetic data.

the M illuminants also yielded results close to the ground truth. In addition, the standard deviations of the 66 initializations is very small for all the fluorescent sheets tested. This indicates that our estimation method is very robust to the choice of initialization values of $\boldsymbol{E}$. Using the average of the RGB values under different illuminants to initialize $\boldsymbol{E}$ is a good choice but almost all other initializations of $\boldsymbol{E}$ would also be just as good.

4. Experimental results

The performance of our method was tested by using images taken by a CCD camera (SONY DXC-9000) under varied illuminants. The types of illuminants used were 9 colored lights ranging from blue to red in the visible spectrum (Figure 4), which were produced by a Nikon Equalized Light Source (ELS).

Scene	R Only		R+F	
	Min	Max	Min	Max
Color Wheel	0.4090	0.5063	0.0283	0.0500
Cup	0.2254	0.3013	0.0224	0.0374
Train	0.3379	0.6351	0.0346	0.0693

Table 2. The errors between the ground truth and the relighted results. "R Only" means only reflectance was considered. The "R+F" means reflectance and fluorescence were considered. "Max" and "Min" correspond to the maximum and minimum errors under 5 different illuminants, respectively.

4.1. Recovery of Spectra

We first evaluate the accuracy of the recovered spectral reflectance and fluorescence absorption and emission spectra of the green and orange fluorescent sheets on the color wheel of Figure 1. Figure 5 shows the recovered spectral reflectance and fluorescence absorption and emission spectra of the green (the left column) and orange (the right column) fluorescent sheets. The recovered spectral reflectance (Figure 5 (a) and (b)), absorption spectra (Figure 5 (c) and (d)) and emission spectra (Figure 5 (e) and (f)) of both fluorescent sheets approximate the ground truth well. We also compared our method against previous work [4]. To allow for the fairest comparison under ideal conditions for both methods, we performed synthetic tests. Compared against [4], which requires a hyperspectral camera and specialized illuminants, we achieve competitive results (Figure 6). Similar results were observed for other spectra as well.

4.2. Relighting Results

Since our method is able to recover the full spectral reflectance, fluorescence absorption, and fluorescence emission spectra for an entire scene, the scenes can be relighted. In this section, we quantitatively evaluate the errors in relighting of real scenes. Figures 7, 8, and 9 show relighting results using the spectral reflectance, fluorescence absorption and emission spectra estimated by our method. We evaluated the accuracy of relighting with our method by computing errors between the ground truth and the relighted results for 3 scenes under 5 illuminants as $\sqrt{\sum_n (p_n^{gt} - p_n^{re})^2 / \sum_n (p_n^{gt})^2}$, where p_n^{gt} is the ground truth (corresponding images in Figures 7-9 (b)) and p_n^{re} is the relighting result (Figures 7-9 (d) and (f)). Table 2 shows the maximum and minimum errors for 3 scenes under 5 illuminants. We can see that the errors are large when only reflectance is considered. When fluorescence is considered, the errors are small and show that the predicted colors are very close to their ground truth images.

Figure 7 also shows the separation of reflectance and fluorescence for a fluorescent scene in addition to relighting results. In Figure 7 (c) and (e) we see the recovered reflective and fluorescent components. In the scene, the notebook on the left only has ordinary reflectance so its colors in the
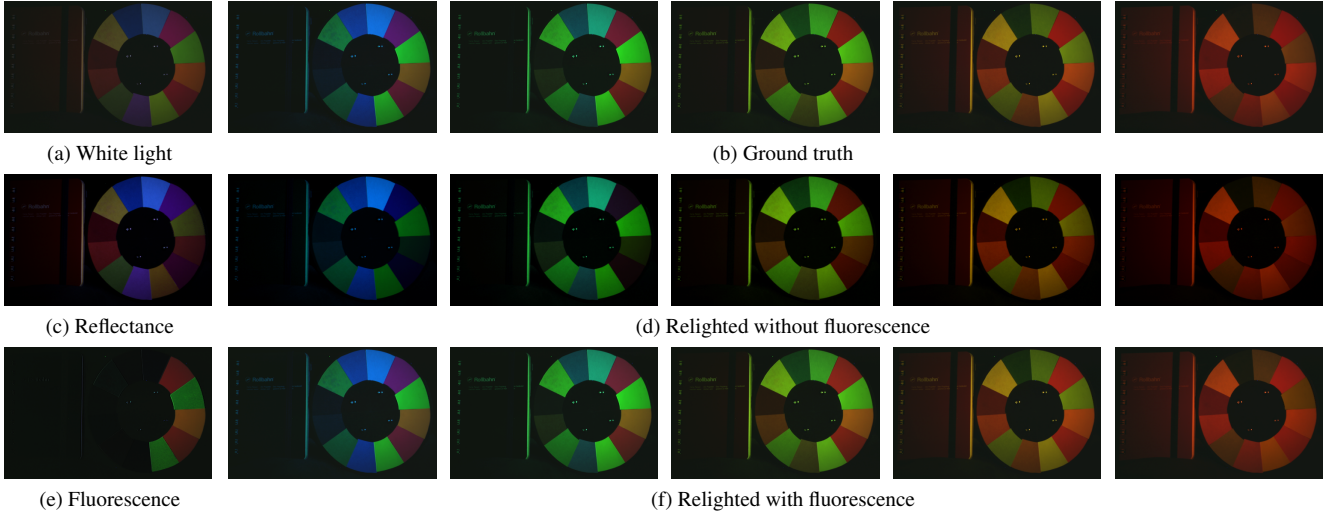
(a) White light

(b) Ground truth

(c) Reflectance

(d) Relighted without fluorescence

(e) Fluorescence

(f) Relighted with fluorescence

Figure 7. Relighting results for the fluorescent color wheel.

(a) White light

(b) Ground truth

(c) Reflectance

(d) Relighted without fluorescence
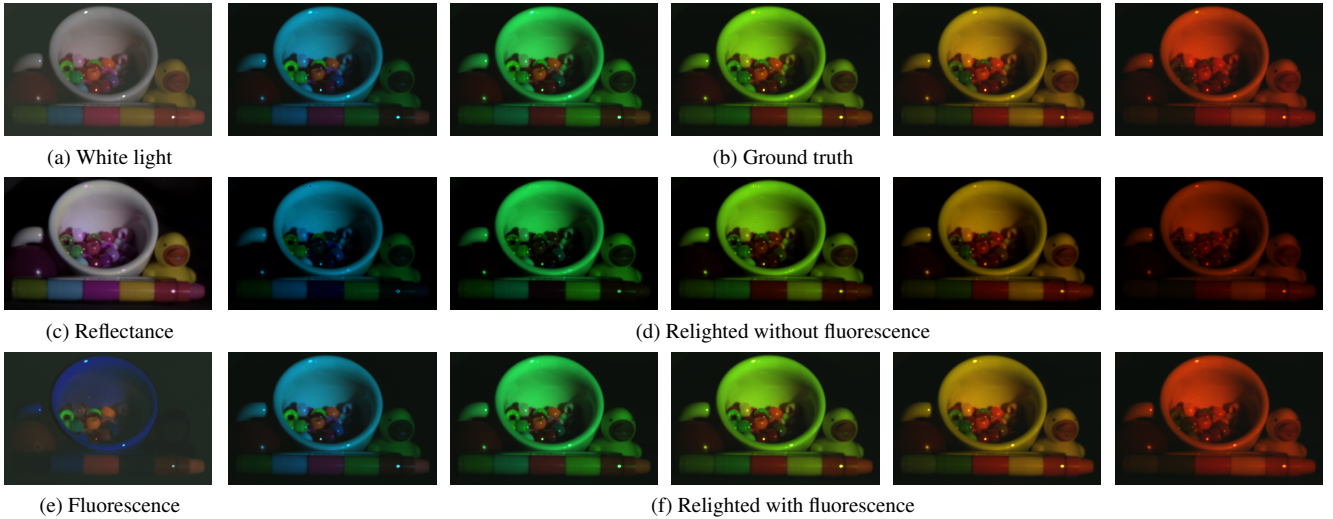
(e) Fluorescence

(f) Relighted with fluorescence

Figure 8. Relighting results for the fluorescent cup scene.

recovered reflective component (Figure 7 (c)) are the same as those seen under white light ((Figure 7 (a)).

The ground truth for the color wheel scene under the 5 illuminants can be seen in Figure 7 (b) and the estimated corresponding relighting results in Figure 7 (f). We can see that, the relighting results are very similar to the ground truth images (Figure 7 (b)) thus demonstrating the effectiveness of our method in recovering the spectral reflectance and fluorescence absorption and emission spectra. When the scene is relighted without considering fluorescent effects in the scene (Figure 7 (d)), this leads to many fluorescent materials appearing as black, especially under blue-green light (the first column in Figure 7 (d)). For the parts of the image that are not black, we can only observe the colors that are present in the illuminant. For example, under blue-green light, Figure 7 (d) only shows blue and green colors. The other results from the second to fifth columns in Figure

7 (d) and Figures 8 and 9 show similar effects.

5. Conclusion

In this paper, we presented a method to simultaneously recover the reflectance and fluorescence absorption and emission spectra of an entire scene by using RGB images under varied illuminants. Making use of the illuminant-invariant chromaticity of fluorescence, our method is capable of estimating the reflectance spectrum and chromaticity of the fluorescent component. Moreover, the fluorescence absorption and emission spectra are estimated accurately by exploiting the basis representation of absorption spectra and a strong correlation between fluorescent chromaticity and emission spectra, respectively. The effectiveness of the proposed method was successfully demonstrated with experiments on real data taken under varied illuminants. In addition, the recovered spectra was used to relight scenes

(a) White light   (b) Ground truth

(c) Reflectance   (d) Relighted without fluorescence

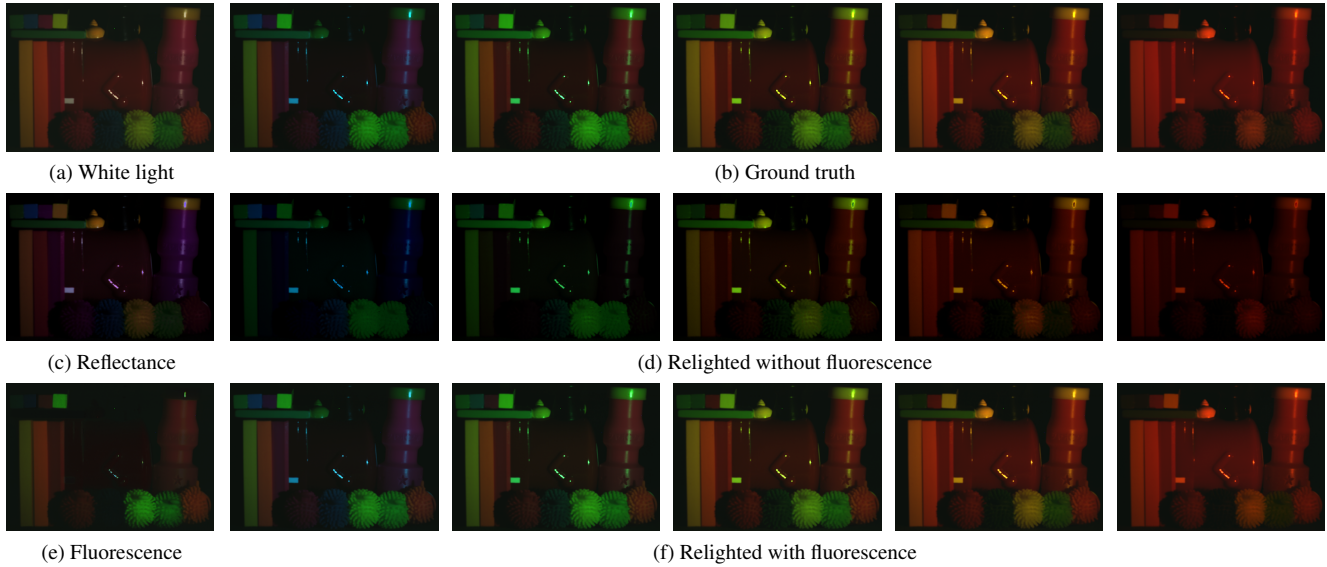(e) Fluorescence   (f) Relighted with fluorescence

Figure 9. Relighting results for the fluorescent train scene.

well. In the future, we plan to extend this method to high speed cameras under fast changing illuminants, so that all these spectra can be recovered for fast moving objects.

References

[1] M. Alterman, Y. Schechner, and A. Weiss. Multiplexed fluorescence unmixing. In *IEEE International Conference on Computational Photography (ICCP)*, 2010.

[2] K. Barnard. Color constancy with fluorescent surfaces. In *CIC,Proceedinds of the IS&T/SID Color Imaging Conference*, 1999.

[3] J. M. DiCarlo, F. Xiao, and B. A. Wandell. Illuminating illumination. In *CIC*, pages 27–34. IS&T/SID, 2001.

[4] Y. Fu, A. Lam, I. Sato, T. Okabe, and Y. Sato. Separating reflective and fluorescent components using high frequency illumination in the spectral domain. In *to appear in IEEE International Conference on Computer Vision (ICCV)*, 2013.

[5] S. Han, Y. Matsushita, I. Sato, T. Okabe, and Y. Sato. Camera spectral sensitivity estimation from a single image under unknown illumination by using fluorescence. In *IEEE Conference on Computer Vision and Pattern Recognition (CVPR)*, 2012.

[6] M. B. Hullin, M. Fuchs, I. Ihrke, H.-P. Seidel, and H. P. A. Lensch. Fluorescent immersion range scanning. *ACM Trans. Graph.*, 27:87:1–87:10, 2008.

[7] M. B. Hullin, J. Hanika, B. Ajdin, H.-P. Seidel, J. Kautz, and H. P. A. Lensch. Acquisition and analysis of bispectral bidirectional reflectance and reradiation distribution functions. *ACM Trans. Graph.*, 29:97:1–97:7, 2010.

[8] J. Jiang and J. Gu. Recovering spectral reflectance under commonly available lighting conditions. In *IEEE Computer Society Conference on Computer Vision and Pattern Recognition Workshops (CVPRW)*, 2012.

[9] G. Johnson and M. Fairchild. Full-spectral color calculations in realistic image synthesis. *IEEE Computer Graphics and Applications*, 19:47–53, Aug. 1999.

[10] A. Lam and I. Sato. Spectral modeling and relighting of reflective-fluorescent scenes. In *IEEE Conference on Computer Vision and Pattern Recognition (CVPR)*, 2013.

[11] J. E. Leland, N. L. Johnson, and A. V. Arecchi. Principles of bispectral fluorescence colorimetry. In *Proc. SPIE*, volume 3140, pages 76–87. SPIE, 1997.

[12] L. T. Maloney and B. A. Wandell. Color constancy: a method for recovering surface spectral reflectance. *JOSA A*, 3(1):29+, 1986.

[13] G. McNamara, A. Gupta, J. Reynaert, T. D. Coates, and C. Boswell. Spectral imaging microscopy web sites and data. *Cytometry. Part A: the journal of the International Society for Analytical Cytology*, 69(8):863–871, 2006.

[14] J. Park, M. Lee, M. D. Grossberg, and S. K. Nayar. Multispectral Imaging Using Multiplexed Illumination. In *IEEE International Conference on Computer Vision (ICCV)*, 2007.

[15] J. P. S. Parkkinen, J. Hallikainen, and T. Jaaskelainen. Characteristic spectra of munsell colors. *Journal of the Optical Society of America A*, 6(2):318–322, 1989.

[16] I. Sato, T. Okabe, and Y. Sato. Bispectral photometric stereo based on fluorescence. In *IEEE Conference on Computer Vision and Pattern Recognition (CVPR)*, 2012.

[17] S. Tominaga, T. Horiuchi, and T. Kamiyama. Spectral estimation of fluorescent objects using visible lights and an imaging device. In *Proceedinds of the IS&T/SID Color Imaging Conference*, 2011.

[18] T. Treibitz, Z. Murez, B. G. Mitchell, and D. Kriegman. Shape from fluorescence. In *European conference on Computer Vision*, pages 292–306, 2012.

[19] A. Wilkie, A. Weidlich, C. Larboulette, and W. Purgathofer. A reflectance model for diffuse fluorescent surfaces. In *International conference on Computer graphics and interactive techniques*, pages 321–331, 2006.

[20] C. Zhang and I. Sato. Separating reflective and fluorescent components of an image. In *IEEE Conference on Computer Vision and Pattern Recognition (CVPR)*, 2011.